Journal of Materials Chemistry A

RSC Publishing

PAPER

View Article Online
View Journal | View Issue

Cite this: J. Mater. Chem. A, 2013, 1, 7433

Mechanically strong graphene oxide/sodium alginate/polyacrylamide nanocomposite hydrogel with improved dye adsorption capacity†

Jinchen Fan, Zixing Shi,* Min Lian, Hong Li and Jie Yin

Received 12th February 2013
Accepted 27th March 2013

DOI: 10.1039/c3ta10639j

www.rsc.org/MaterialsA

In this paper, a novel graphene oxide (GO)/sodium alginate (SA)/polyacrylamide (PAM) ternary nanocomposite hydrogel with excellent mechanical performance has been fabricated through free-radical polymerization of acrylamide (AAm) and SA in the presence of GO in an aqueous system followed with ionically crosslinking of calcium ions. As-prepared GO/SA/PAM (weight ratio SA : AAm = 1 : 2) ternary nanocomposite hydrogel with 5 wt% of GO displays a compressive stress as high as 1.543 MPa at the compressive deformation of 70%. The tensile strength and modulus of the hydrogel achieved ~201.7 and ~30.8 kPa, respectively. In the meantime, the ternary nanocomposite hydrogels can recover a large proportion of elongation at breakage and exhibits good elasticity. Additionally, the GO/SA/PAM ternary nanocomposite hydrogel exhibited good adsorption properties for water-soluble dyes. After introducing GO, the dye adsorption capacities of the hydrogel were significantly improved.

1 Introduction

Hydrogel, a three-dimensional network of hydrophilic polymers, can swell in water and hold a large amount of water while maintaining its structure. It is formed by crosslinking of polymer chains by covalent bonds, hydrogen bonding, van der Waals interactions, or physical entanglements. Due to its unique properties, hydrogels were applied in a drug delivery system (DDS), biomedical and tissue engineering, *etc.*[1–3] However, most of the hydrogels suffer from a lack of mechanical performance. The poor mechanical property of hydrogel has often limited its further industrial and biomedical applications.[4,5]

Recently, a lot of research work has been devoted to improving the mechanical performance of hydrogels.[6,7] Composite hydrogels are considered to be a simple way of improving the mechanical properties of hydrogels with the addition of reinforcing organic/inorganic fillers such as clay, cellulose, carbon nanotubes, *etc.*[8–10] Graphene and graphene oxide (GO) have been attracting tremendous attention as nanofillers for polymer reinforcement due to their large theoretical specific surface area.[11] GO has a large number of oxygen-containing groups, such as hydroxyl, epoxide and carboxyl groups.[12] As a result, it makes GO hydrophilic, readily dispersible in water as well as other solvents, and easily modified to be compatible with polymer for enhancing the mechanical performance of hydrogel.[13–16] Zhang *et al.* and Liu *et al.* introduced GO into the networks of polyacrylamide (PAM) hydrogel. The results demonstrated that GO can be well dispersed in the GO/PAM hydrogel and consequently contributed to a significant improvement of their mechanical properties.[17,18] He *et al.* prepared GO/SA hydrogel fibers using a wet-spinning method, in which a calcium chloride solution was used as a coagulation bath. For GO/SA hydrogel fibers cross-linked by Ca^{2+} ions, the incorporation of GO significantly improved the tensile strengths of the GO/SA hydrogel fibers owing to the uniform distribution of the layered GO in the SA matrix.[19]

In fact, there are three types of hydrogels with good mechanical performance which have been developed: a 'topological (TP) gel', a 'nanocomposite (NC) gel', and a 'double network (DN) gel'.[7] Amongst these, the DN hydrogel, comprising two independently cross-linked networks, is commonly considered as an effective method for fabrication of mechanically strong hydrogels.[6,20] Sodium alginate (SA), natural polysaccharide extracted from brown seaweed, has been widely used in the wound management industry as a novel material for the manufacture of 'moist healing' products such as gels, foams and fibrous.[21] It can form hydrogels in the presence of divalent cations (such as Ca^{2+}) due to ionic cross-linking *via* calcium bridges between the mannuronic acid (M unit) and guluronic acid (G unit) on adjacent chains.[22,23] Sun *et al.* synthesized SA/PAM hydrogel by introducing the SA into the networks of PAM hydrogel. The SA/PAM DN hydrogel from ionically cross-linked alginate and covalent crosslinked PAM networks were highly stretchable and tough.[24]

School of Chemistry and Chemical Engineering, State Key Laboratory for Metal Matrix Composite Materials, Shanghai Jiao Tong University, 200240, Shanghai, People's Republic of China. E-mail: zxshi@sjtu.edu.cn; Fax: +86 21 54747445; Tel: +86 21 54743268

† Electronic supplementary information (ESI) available. See DOI: 10.1039/c3ta10639j

As mentioned above, the addition of reinforcing fillers and the introduction of new cross-linked networks were both considered to be effective methods for improving the mechanical performance of the hydrogel. If the two methods were combined together, the mechanical properties of hydrogels should be significantly improved and better than the reinforced hydrogel with the addition of reinforcing fillers or the introduction of new cross-linked networks respectively. In other words, addition of the reinforcing filler in DN hydrogels can further improve the mechanical performance of the hydrogel.

Based on this consideration, the GO/SA/PAM (GSP) ternary composite hydrogels were prepared by introducing GO into the SA/PAM (SP) hydrogel followed by ionically crosslinking of calcium ions. The layered GO were inserted into the networks of Ca^{2+} crosslinked alginate and covalent crosslinked PAM of SA/PAM hydrogel. Compressive and tensile tests of the GSP hydrogel were used to study its mechanical properties. In the meantime, the dye adsorption abilities of the composite hydrogels were also investigated.

2 Experimental

2.1 Materials

Graphite powder (100 meshes, 99.9995%) was obtained from Alfa-Aesar Co., Ltd SA, AM, ammonium persulfate (APS), *N*,*N*′-methylenebisacrylamide (MBA), potassium permanganate ($KMnO_4$), concentrated sulfuric acid (95–98%), hydrogen peroxide (H_2O_2, 30%), concentrated hydrochloric acid, calcium chloride hydrate ($CaCl_2 \cdot 2H_2O$) and all organic solvents were purchased from Sinopharm Chemical Reagent Co. Ltd (SCRC) and used as received. The dyes, brilliant green (BG), methyl orange (MO), bordeaux red (BR), rhodamine 6G (R6G), calcein (CA), malachite green (MG), methylene blue (MB) and rose bengal sodium salt (RB), were also purchased from SCRC. Other reagents used were all analytical grade and all solutions were prepared with deionized (DI) water.

2.2 Preparation of the GSP ternary composite hydrogels

Graphite oxide was obtained by using the modified Hummers method from graphite.[25,26] Hydrogels were prepared by a simple mixture and solution polymerization using initial solutions consisting of monomers (GO, SA and AAm), crosslinker (MBA), initiator (APS). Firstly, the desired amount of dried GO was first exfoliated and dispersed in 10 mL of water by sonication for 3 h. Successively, SA and AAm were added and dissolved in the GO aqueous dispersion of 10 mL under magnetic stirring for 3 days at room temperature. The GO/SA/AM mixture solutions were kept at 0 °C, and then 0.02 g of APS and 0.03 g MBA was added. After magnetic stirring for 2 hours under 0 °C, the homogeneous mixture solutions were transferred into a glass tube and kept for hydrogel formation at 80 °C for 2 h. After hydrogel formation, the GSP ternary composite hydrogels, in its cylindrical form, were taken out of the glass tube and put into DI water for removing homopolymers and unreacted monomers. The water was renewed every 8 h for 1 week. In this paper, hydrogels are expressed as S*m*P*n*, G*x*P*n*, and G*x*S*m*P*n* gels, where S, P and G stand for hydrogels containing sodium alginate, polyacrylamide and graphene oxide respectively, and *m*, *n* and *x* represent the feed amounts of SA, AAm and the relative weight ratio of GO to the total amount of SA and AAm. For examples, the G5S1P2 hydrogel implies that there are 1.0 g of SA, 2.0 g of AAm and 150 mg of GO (account for 5 wt% of total amounts of SA and AAm) in the feeding amounts of hydrogel preparation. SA itself can form hydrogels in the presence of Ca^{2+} ions due to ionic cross-linking *via* calcium bridges between the mannuronic acid (M unit) and guluronic acid (G unit) on adjacent chains. Successively, among of S*m*P*n*, G*x*P*n*, and G*x*S*m*P*n* hydrogels, the S*m*P*n* and G*x*S*m*P*n* hydrogels were continue to be immersed into the 4 wt% $CaCl_2$ aqueous solution with Ca^{2+} ionically crosslinking for 24 h. Finally, the hydrogels continued to be placed into DI water again for 1 week with a water-change every 8 h.

2.3 Instruments and characterizations

Fourier transform infrared spectroscopy (FTIR) spectra were recorded on a Perkin-Elmer Paragon 1000PC spectrometer. X-ray powder diffraction (XRD) patterns were recorded on a D/max-2200/PC (Japan Rigaku Corp.) using Cu Kα radiation (λ = 1.5418 Å). Differential scanning calorimetry (DSC) was carried out using a TA instrument (Q2000, TA Instruments) at a heating rate of 10 °C min^{-1}, under nitrogen flux. Ultraviolet visible (UV-Vis) absorption spectra were recorded by UV-2550 spectrophotometer (Shimadzu, Japan). Atomic Force Microscope (AFM) images were obtained by digital E-Sweep Atomic Force Microscope in tapping mode. The morphology of GO were obtained by using transmission electron microscopy (TEM) (JEOL2100F). The network structures of hydrogels were characterized by scanning electron microscopy (SEM) (JSM-7401F).

2.3.1 Compressive tests of hydrogels. For compressive test, the hydrogels were prepared in a glass tube with a diameter of 24 mm and a length of 20 cm. The obtained hydrogels for compressive tests, in its cylindrical form, were tested in equilibrium swelling state. Using an Instron 4465 instrument, the measurement of compressive tests were performed on the cut hydrogels with a height of 4 cm. The conditions of the compressive tests are listed as follows: crosshead speed of 1 cm min^{-1}, a load cell of 2 kN, temperature of 25 °C, initial gauge length of 40 mm and final gauge length of 10 mm.

2.3.2 Tensile tests of hydrogels. Similar to the compressive tests, the tensile tests of hydrogels were also performed in the equilibrium swelling state. However, the hydrogel samples were formed in the glass tube with a diameter of 6 mm and a length of 10 cm. The tensile tests were also performed on an Instron 4465 instrument. The conditions of the tensile test are listed as follows: crosshead speed of 6 mm min^{-1}, a load cell of 2 kN, temperature of 25 °C, initial gauge length of 40 mm.

2.3.3 Rheological property measurements. Rheological properties of PAM, S1P1, and G5S1P2 hydrogels were conducted with TA ARES-G2 rheometer using parallel plates of diameter 20 mm at 25 °C. The gap between the two parallel plates was set at 1 mm. First, the dynamic strain sweep from 0.01% to 100% was carried out at an angular frequency of 1 Hz. Then, the

frequency sweep was performed over the frequency range of 0.001–20 Hz at a fixed strain of 0.5%.

2.3.4 Equilibrium swelling degree of hydrogel. For determining the equilibrium swelling degree (ESD) of hydrogels, the as-prepared hydrogels were first lyophilized in freeze-drying equipment for 1 week. Then, certain amounts of dried hydrogels were immersed into the DI water until the hydrogels achieved an equilibrium swelling state in sealed containers at room temperature for 1 week. Afterwards, the equilibrium swollen hydrogels were taken out, after removal of excess surface water with a filter paper, and weighed. The ESD is calculated from the equation:[27,28]

$$\mathrm{ESD} = \frac{W_e - W_d}{W_d},$$

where W_e and W_d represent the weights of the dried hydrogel and the hydrogel at swelling equilibrium state, respectively.

2.3.5 Dye adsorption of hydrogels. Desired amounts of dried hydrogels were first put into the DI water until the equilibrium swelling states were achieved. A variety of water-soluble dyes were used to test the dye adsorption capacities of the hydrogels, and the dyes dissolved in deionized water to form solutions with a fixed concentration. Then the equilibrium swollen hydrogels were added into the dye aqueous solutions, and the dye adsorption experiments were performed at 25 °C for 1 week until adsorption equilibrium was achieved. The concentrations of the dye aqueous solutions before and after adsorption were measured by ultraviolet spectrophotometry at the maximum absorption wavelength (λ_{max}) of the corresponding dye.

The equilibrium adsorption capacity, Q_e (mg g^{-1}), was calculated by the equation:[29,30]

$$Q_e = \frac{C_0 V_{dye} - C_e V_{dye}}{M_{dh}},$$

where C_0 and C_e (mg mL^{-1}) are the initial and final concentrations of the dye solution. V_{dye} (mL) and M_{dh} (g) are the volume of the dye solution and the weight of dried hydrogel, respectively.

3 Results and discussion

Graphite oxide was obtained by oxidation of graphite using a modified Hummers method.[25,26] Due to the oxygen-containing groups on its basal plane and edges, graphite oxide can be exfoliated to GO nanosheets in aqueous solution with sonication. As shown in Fig. 1a, the XRD pattern of GO shows an evident peak at $2\theta = 9.41°$, corresponding to a *d*-spacing of 0.94 nm, due to the inter-lamellar water trapped between GO nanosheets.[12] In Fig. 1b, the C1s XPS spectrum of GO nanosheets indicates a considerable degree of oxidation with four components that correspond to carbon atoms in different functional groups of the non-oxygenated ring C, the C in C–O bonds, the carbonyl C=O, and the carboxylate carbon (O–C=O).[31,32] By the elemental analysis, the C/O ratio of GO nanosheets was 1.67/1. Fig. 1c and d depict the typical AFM and TEM images of the obtained layered GO nanosheets. The thickness, determined from the height profile of the AFM image, Fig. 1d, is around ~0.57 nm, which is consistent with the data reported in the literature, indicating the formation of single layered GO.[33]

Since graphite oxide can be thoroughly exfoliated in water, it is very suitable to be used in preparation of nanocomposite hydrogels.[34,35] GO nanosheets can be well dispersed in the SA and AAm aqueous solution respectively.[17–19] Moreover, we found that GO can also be well dispersed in the mixture solution of SA and AAm and formed uniform solutions. The *in situ* polymerization technique is attractive since it enables control over both the polymer architecture and the final structure of the composites.[34–36] The GSP ternary composite hydrogels were prepared by a simple mixture and *in situ* polymerization using initial solutions consisting of monomers (GO, SA and AAm), crosslinker (MBA), initiator (APS). After hydrogel formation, the nanocomposite hydrogels were immersed into the 4 wt% $CaCl_2$ aqueous solution for ionically crosslinking. It is clearly seen from Fig. S1† that the GO nanosheets were uniformly distributed in the ternary nanocomposite hydrogels. With increasing the amount of GO, the colors of the hydrogels gradually darken.

From Fig. 2a–c, the pure PAM hydrogel was damaged after compression under pressure. However, the G5S1P2 ternary nanocomposite hydrogel displays high performance in ductility. From Fig. 2d–f, the G5S1P2 hydrogel was not damaged after compression under pressure. Upon removing of the compression force, G5S1P2 hydrogel fast recovered its original cylinder shape. The G5S1P2 hydrogel also can bounce repeatedly and skip on the surface of glass (see ESI, Movie S1†). The results showed that the G5S1P2 hydrogel was very flexible and elastic.

Compressive and tensile tests were both used to characterize the mechanical properties of the hydrogels. As shown in Fig. 3, the PAM hydrogel was broken when the compressive strength reached ~0.0058 MPa at the compressive deformation of ~35%. After introduction of GO nanosheets, the compressive strength of the G5P3 hydrogel increased to ~0.164 MPa at the compressive deformation of ~70%. In fact, the SA/PAM exhibits high stretchability and strength.[24] From Fig. 3, the compressive strength of S1P2 hydrogel is ~0.905 MPa, ~156 times more than that of PAM hydrogel. The compressive strength of the G5S1P2 hydrogel with 5 wt% of GO achieved at ~1.543 MPa, increased by ~70.5% compared to the S1P2 hydrogel. Table 1 reflects the mechanical performance of PAM, G5P3, S1P2 and G5S1P2 hydrogels. From Table 1, the introduction of SA and addition of GO both improved the mechanical performance of the hydrogel. Furthermore, combining the SA and GO into the PAM hydrogel by *in situ* polymerization followed with Ca^{2+} ions crosslinking, the strength and modulus of G5S1P2 hydrogel were superior to the G5P3 and S1P2 hydrogels.

Obviously, the introduction of GO into the SP hydrogels can further improve their mechanical properties. For GP binary nanocomposite hydrogels, the oxygen-containing groups of GO participated in radical chain transfer reactions during the free-radical polymerization, leading to the grafting of PAM macromolecules onto the layered GO sheets. As a result, the GO nanosheets acted as fresh chemical crosslinking points in

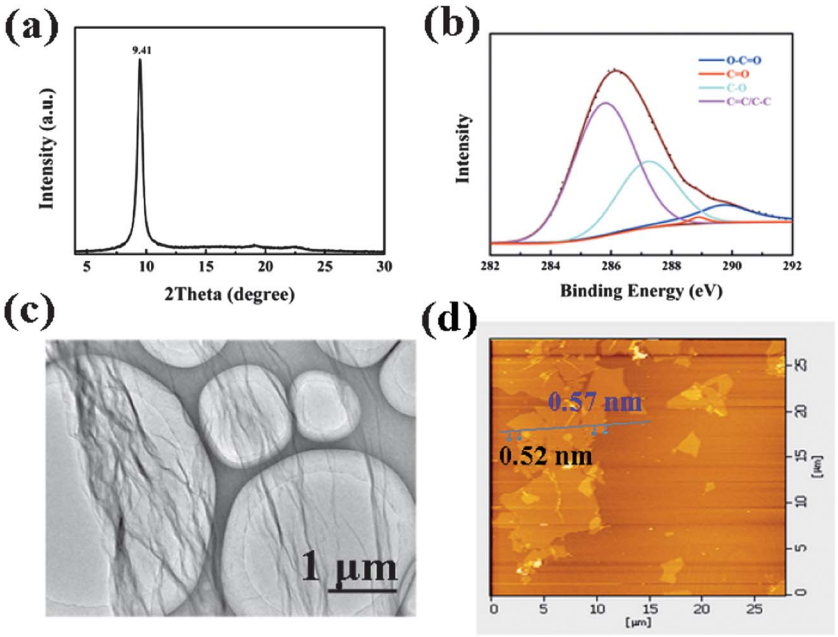

Fig. 1 (a) The XRD pattern of GO, (b) the C1s XPS spectrum for GO, (c) TEM image of GO and (d) AFM image of GO.

hydrogel formation.[14,17] Moreover, the Ca^{2+}-crosslinked SP DN hydrogels are also highly stretchable and tough. It is mainly attributed to the synergy of calcium bridging by the network of covalent crosslinks and hysteresis by unzipping the network of ionic crosslinks.[24] Taken together, the introduction of GO into the SP DN hydrogels further improved their mechanical properties. The schematic diagram of GSP ternary nanocomposite hydrogel was illustrated in Fig. 2g. The layered GO nanosheets were intercalated with the polymer networks of hydrogel. The load transfer between the polymer chains of hydrogel and GO nanosheets is beneficial for mechanical improvement of the hydrogel due to the large surface area of the GO nanosheets. There are two types of crosslinked polymer: ionically (Ca^{2+}) crosslinked SA and covalently crosslinked PAM in the network structure of SP hydrogel. When the GO nanosheets were introduced into the SP hydrogel, the new chemical crosslinking points comes from GO nanosheets were produced in the structure of GSP hydrogel. Additionally, the functional groups of GO nanosheets also offer hydrogen bonding with polymer chains. As a result, the GO nanosheets can act as reinforcing nanofillers for further enhancing the mechanical performance of the SP hydrogel.

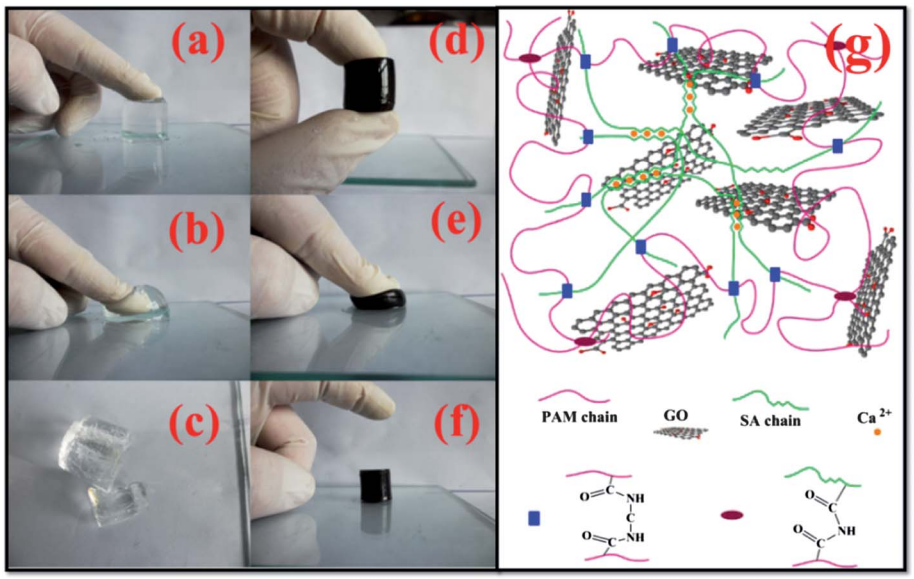

Fig. 2 (a–f) Photographs of PAM and G5S1P2 hydrogels under pressure, (g) schematics of GO/SA/PAM ternary composite hydrogels.

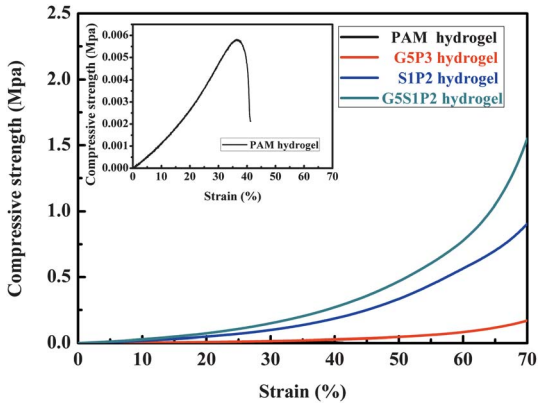

Fig. 3 Typical compressive strain–stress curves of PAM, G5P3, S1P2 and G5S1P2 hydrogels (inset: high-resolution strain–stress curve of PAM hydrogel).

Table 1 Mechanical properties of PAM, G5P3, S1P2 and G5S1P2 hydrogels

Hydrogel sample	Tensile strength (kPa)	Elongation (%)	Modulus (kPa)
PAM	8.4 ± 1.6	254 ± 15	3.9 ± 1.2
G5P3	81.4 ± 2.3	1086 ± 25	13.9 ± 2.8
S1P2	112.8 ± 7.8	817 ± 12	19.9 ± 3.6
G5S1P2	201.7 ± 9.1	592 ± 27	30.8 ± 3.9

For systematically studying the enhancement effect of GO nanosheets for the mechanical performance, the G0.5S1P2, G1S1P2, G2S1P2, G3S1P2, G4S1P2 and G5S1P2 hydrogels with different amounts of GO were prepared. Holding the amount of AAm and SA constant at 2.0 and 1.0 g, the compressive and tensile strengths both increased with the increase of GO (Fig. 4). For the compressive test, the elastic moduli can be calculated from the compressive stress–strain curve.[37] As shown in Fig. 4a, with increasing the amount of GO, the elastic moduli increased from ~127.5 kPa of G0.5S1P2 hydrogel to ~202.3 kPa of G5S1P2 hydrogel. Additionally, the mechanical properties of the hydrogels with different feed amounts of SA and AAm at the same addition of 5 wt% GO were also investigated (Fig. 4c and d). For the SP hydrogel, the introduced chains of Ca^{2+} cross-linked with SA play an important role in its mechanical performance. The amount of SA greatly affects the mechanical performance of SP hydrogel. Obviously, introducing the same amount of GO improved the mechanical performance of SP hydrogel with different feed amounts of SA and AAm. As shown in Fig. 4c and d, the compressive and tensile strengths of the SA/PAM hydrogel increased rapidly from ~156.8 and ~11.76 kPa to ~905.7 and ~113.06 kPa with different amounts of SA.

Sun *et al.* demonstrated that the SP hydrogels were outstandingly stretchable and tough.[24] The SP hydrogel exhibits high elasticity. Fig. 5a and b show the tensile stress–strain and elongation–recovery curves of GSP hydrogels. From Fig. 5a, an increase in tensile strength for GSP hydrogel is accompanied by a decrease in the elongation at breakage of the GSP hydrogel. GO nanosheets can effectively cross-link the polymer chains of hydrogel through surface grafting and hydrogen interaction. The increase of GO content resulted in an increase in cross-linking. Even so, the G5S1P2 hydrogel still maintained good ductility with about 3 times higher than the PAM hydrogel in elongation at breakage. In the meantime, as shown in Fig. 5b, the elongation–recovery curves demonstrated that the GSP can recover a large proportion (~70%) of elongation at breakage. There is scant evident residual strain in the elongation–recovery. It is attributed to the high aspect ratio of GO nanosheets and the strong hydrogen-bonding interaction between GO and PAM.[38,39] Upon loading, the stress can transfer from the flexible polymer chains to GO nanosheets *via* the interface.[40] Similar to the GO/PAM hydrogel, PAM chains can be initiated on the surface of GO nanosheets in GSP hydrogel formation. The dispersed PAM-grafted GO nanosheets are formed in the GSP nanocomposite hydrogels.[14,17] As a result, the polymer chains can be well stretched during tensile testing. After unloading the stress, the GSP hydrogels can be returned to their initial shape with almost no permanent deformation. The results indicated the good elasticity of the GSP hydrogel.

GO can act as an effective reinforcing filler for enhancing the mechanical performance of the hydrogel. In the meantime, with introduction of GO, the GSP nanocomposite hydrogel still keeps its good elasticity. The GSP nanocomposite hydrogels were fabricated through free-radical polymerization of AAm and SA in the presence of GO in aqueous system followed with calcium ions crosslinking. The layered GO nanosheets were dispersed and inserted into the hydrogel networks. On the one hand, the oxygen-containing groups of GO participated in radical chain transfer reactions and the PAM chains were grafted onto the surfaces and edges of GO nanosheets. On the other hand, the functional groups of GO also offer hydrogen bonding with polymer chains.

FT-IR spectra were first used to characterize the interaction between GO and the polymer chains of the hydrogel. As shown in Fig. 6, the characteristic vibrations of GO are the broad and intense peak of O–H groups centered at 3400 cm^{-1}, strong C=O peak at 1737 cm^{-1}, the O–H deformation peak at 1390 cm^{-1}, the C–OH stretching peak at 1228 cm^{-1}, and the C–O stretching peak at 1044 cm^{-1}.[41] In the spectra of SA, the broad band at 3434 cm^{-1} corresponds to hydroxyl groups, the peaks near 1620 and 1411 cm^{-1} were caused by symmetric and asymmetric stretching vibrations of COO^- groups, respectively.[42] The peak around 1666 cm^{-1} is ascribed to the in plane deformation vibration of N–H bond for the S1P2 hydrogel. After introduction of GO, the peak shifts to a higher wavenumber for GSP hydrogel. Additionally, increasing with the content of GO, the shift of the peak at 1666 cm^{-1} becomes more apparent. The shift is attributed to the presence of the hydrogen bonding interactions between the N–H bond of PAM and O–H bond of GO nanosheets.[43,44]

To further understand the hydrogen bonding interaction, XPS measurements for PAM, S1P2 and G5S1P2 hydrogel were performed. Fig. 7a shows the XPS spectra of nitrogen atom for PAM, S1P2 and G5S1P2 hydrogels. The binding energies for nitrogen atoms for dried PAM hydrogel and S1P2 hydrogel are 402.5 and 402.4 eV. But for G5S1P2 hydrogel, the binding energy for nitrogen atoms was decreased to 402.0 eV. It is attributed to the formation of strong hydrogen bonding interactions between the N–H bond of PAM and O–H bond of GO nanosheets as

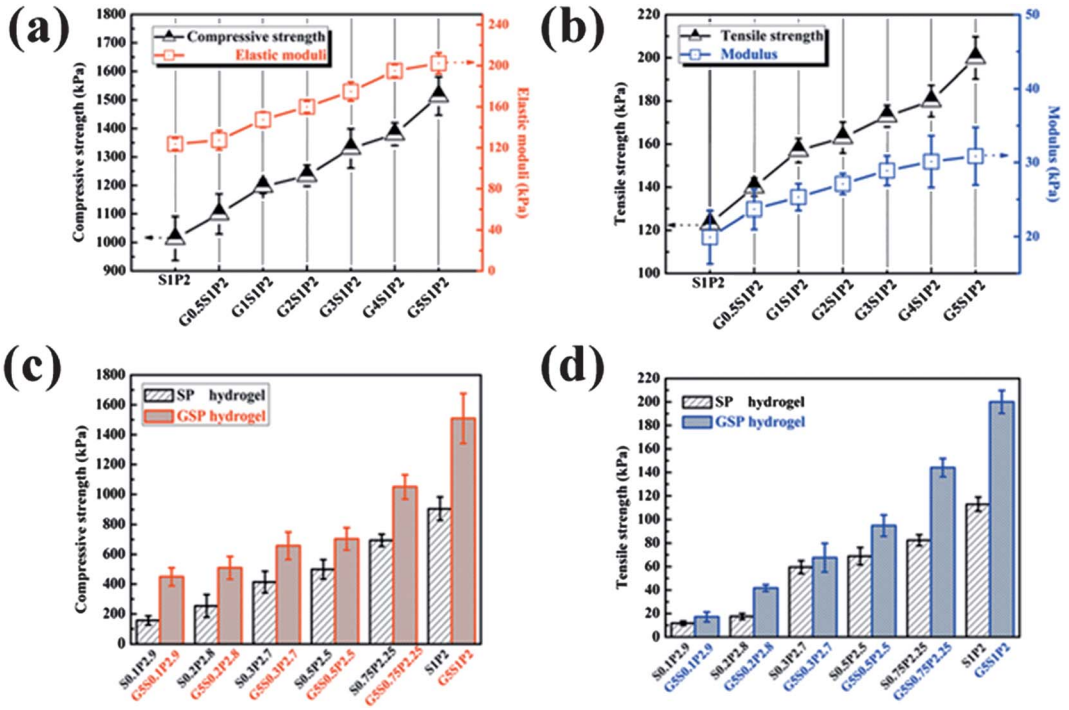

Fig. 4 (a) Compressive strengths and elastic moduli of S1P2, G0.5S1P2, G1S1P2, G2S1P2, G3S1P2, G4S1P2 and G5S1P2 hydrogels, (b) tensile strengths and modulus of S1P2, G0.5S1P2, G1S1P2, G2S1P2, G3S1P2, G4S1P2 and G5S1P2 hydrogels, (c) compressive strengths of the SP and G5SP hydrogels with different feed amounts of SA and AAm and (d) tensile strengths of the SP and G5SP hydrogels with different feed amounts of SA and AAm.

shown in the FT-IR results above.[45] Additionally, the peak for C1s of PAM hydrogels can be deconvoluted into three peaks at 290.6, 287.9 and 287.2 eV, which are assigned to the O═C–N, C–N and C–H species of PAM respectively. These peaks can also be identified in S1P2 and G5S1P2 hydrogels. For G5S1P2 hydrogel, two new peaks appear at 289.6 and 288.5 eV, which are ascribed to the C–O bonds from GO and carbon of carbonate-type species from the interactions between PAM and GO nanosheets.[38] By contrast, the intensity of the peak of O═C–N at 290.6 eV was reduced obviously after introduction of SA and GO. The formation of hydrogen bonding between the N–H bond of PAM and the O–H bond of GO nanosheets is also implied.

Consequently, the XPS and FTIR results confirmed hydrogen bonding interaction in the GSP hydrogel. Towards the SP hydrogel, there are two types of crosslinked polymer: ionically (Ca^{2+}) crosslinked SA and covalently crosslinked PAM. The two types of crosslinked polymer are intertwined, and joined by covalent crosslinks. When the GO nanosheets was introduced into the SP hydrogel, the appearance of crosslinking points for GO and hydrogen bonding interaction between the N–H bond of PAM and O–H bond of GO nanosheets make the GSP hydrogel strong. The load transfer between the polymer chains of hydrogel and GO is also beneficial for mechanical improvement of the hydrogel. SEM images were used to characterize the

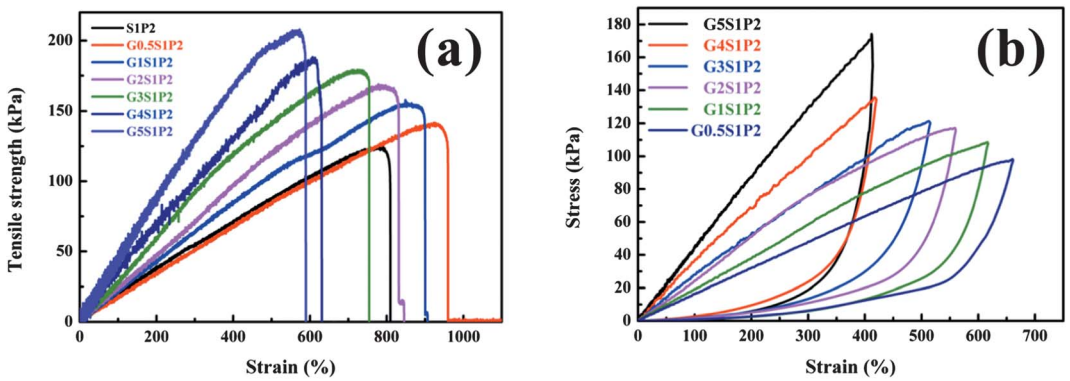

Fig. 5 (a) Typical tensile strain–stress curves of S1P2, G0.5S1P2, G1S1P2, G2S1P2, G3S1P2, G4S1P2 and G5S1P2 hydrogels, (b) the tensile strain–stress curves for elongation–recovery of G0.5S1P2, G1S1P2, G2S1P2, G3S1P2, G4S1P2 and G5S1P2 hydrogels.

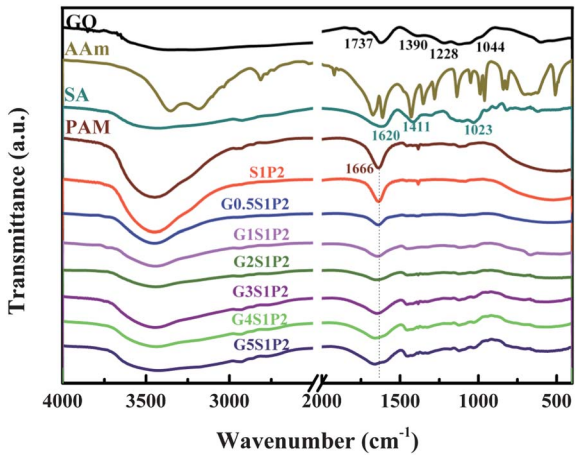

Fig. 6 FTIR spectra of GO, AAm, SA, PAM and S1P2 hydrogels with different amounts of GO.

structure of GSP ternary composite hydrogel. As shown in Fig. 8, it can be clearly seen that the hydrogel samples show a sponge-like architecture with pore diameters at the micrometric level. From Fig. 8a–c, the holes of PAM and S1P2 hydrogels are uniformly distributed over a large scale. After introduction of GO, the morphologies of the hydrogels were changed. From Fig. 8d–f for GO/PAM composite hydrogel, there are filamentous structures with interconnecting pores inside and outside the holes of the hydrogel. It is attributed to the layered GO participating in the formation of the network structures. In Fig. 8d–f, after addition of GO, the large hole structures of the S1P2 hydrogel were replaced by a structure of combining lamellar and net structures. It is worth noting that the structures of the G5S1P2 hydrogel become more dense. The GO were inserted into the networks of the hydrogel and resulted in the lamellar structure. The density structures of G5S1P2 hydrogel were contributed to the further improvement of the mechanical performance for hydrogels.

Due to the high surface area of GO nanosheets and the interfacial interactions in the hydrogel, the dynamic viscoelastic properties of the hydrogels were examined in a dynamic stress environment by a rheometer. Fig. 9a shows the shear modulus (G') curves of PAM, S1P2 and G5S1P2 hydrogels as a function of strain. The absolute value of shear modulus for S1P2 hydrogel increased after introduction of GO nanosheets, consistent with the previous compressive and tensile tests of the hydrogels. Towards 1% of strain, the G' for G2S1P2 hydrogel is ~22 152 Pa. When the amount of GO increased to 5 wt%, the G' reached to ~35 135 Pa, which is ~58.6% higher than the G2S1P2 hydrogel. Increasing with the strain, the shear modulus sharply decreased due to the relatively loose structure of GO nanosheets inserted in the hydrogel being destroyed by the higher stress.[38,46] The frequency sweeping results also demonstrated the reinforcing effect of GO nanosheets. From Fig. 9b, the shear moduli (G') were increased at the frequency range from 0.1 to 10 Hz after

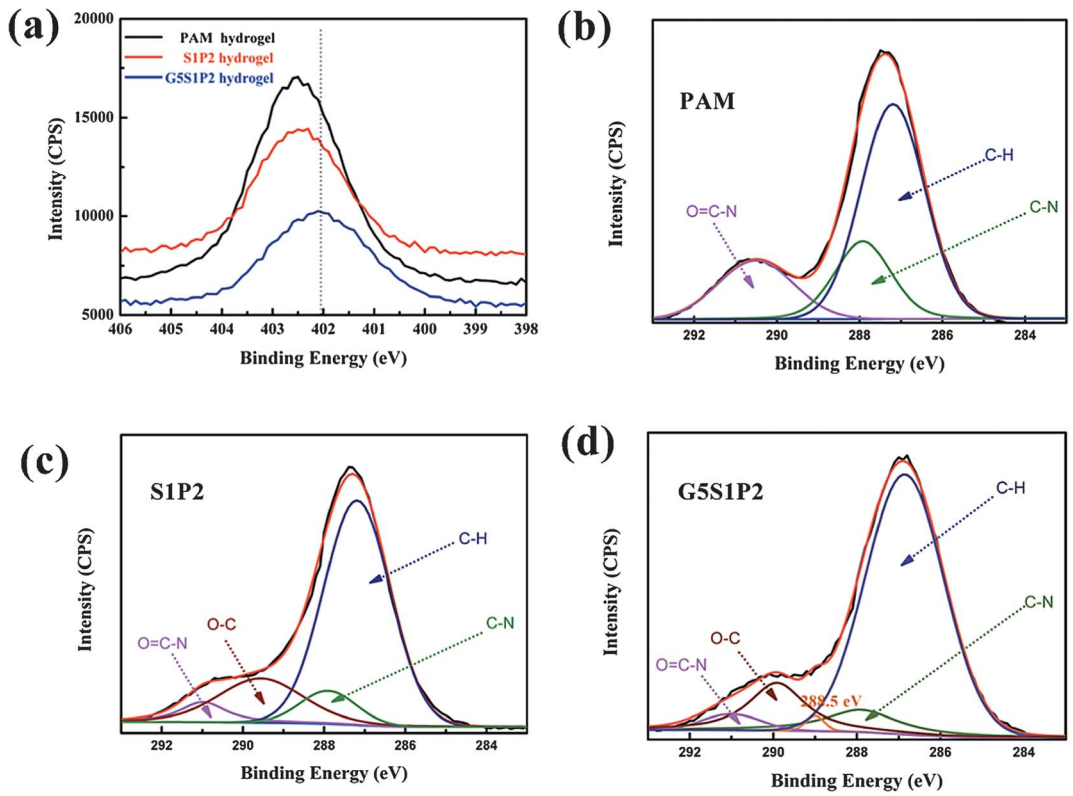

Fig. 7 (a) High-resolution XPS spectra of nitrogen atom for PAM, S1P2 and G5S1P2 hydrogels, (b) carbon atom for PAM hydrogel, (c) carbon atom for S1P2 hydrogel, and (d) carbon atom for G5S1P2 hydrogel.

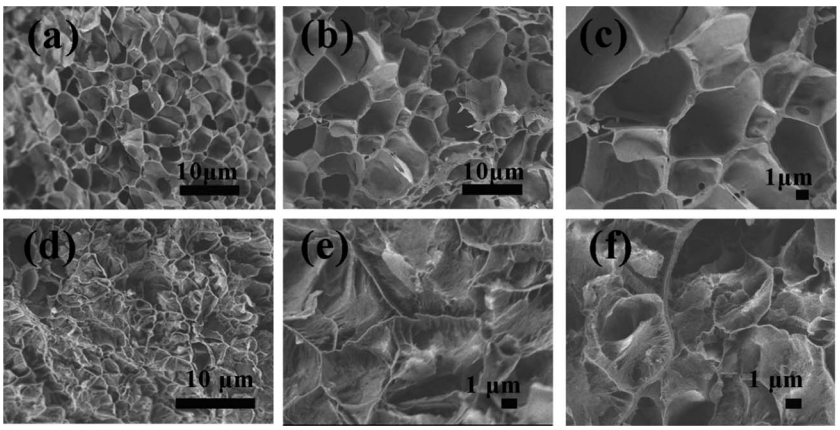

Fig. 8 SEM images of the hydrogels, (a) PAM hydrogel, (b) S1P2 hydrogel, (c) a local partial enlarged image of (b), (d) G5S1P2 hydrogel, and (e and f) local partial enlarged images of (d).

introduction of GO nanosheets. At the 1 Hz of frequency, the shear modulus of G5S1P2 is ~31 115 Pa, higher the PAM, S1P2, and G2S1P2. In all, the dynamic viscoelastic properties further suggest the excellent reinforcing effect of GO nanosheets in SP hydrogel.

With introduction of GO, the increase of crosslinking points greatly restrict the motion of macromolecular chains and result in an increase in their glass transition temperature. From Fig. 10a, the T_g of the PAM hydrogel was around 85.8 °C. When the GO inserted the networks of PAM, the T_g raised from 85.8 to 90.1 °C for G5P3 with 5 wt% of GO. Additionally, for the SA/PAM hybrid hydrogel, the T_g was also improved from 88.6 °C of S1P2 to 94.5 °C of G5S1P2 after introduction of 5 wt% of GO. After introduction of GO, the layered GO nanosheets were inserted into the network structure of the hydrogel and restrict the motion and transfer of polymer chains.[14,47] The capacity of swelling is one of the most important parameters to evaluate the structures of hydrogels. Equilibrium swelling degrees (ESD) of the hydrogels in distilled water at the room temperature were also investigated. In Fig. 10b, with increasing amounts of SA, the ESD of the SP hydrogel decreased gradually. It is attributed to the SA chains being introduced into the network structure of the hydrogel. Due to the Ca^{2+} ionically SA crosslinks and covalent crosslinks between amine groups of PAM chains and carboxyl groups of SA chains, with increasing SA amount, the high degree of crosslinking contributed to the reduction of ESD. To better understand the influence of the GO on the swelling behavior, the ESD for GS1P2 with different amounts of GO were measured and the results are shown in Fig. 10c. When GO is incorporated into the SP hydrogel, the ESD of GSP decreased and larger amounts of GO caused a larger swelling decrease.

3.1 Dye adsorption of the GO/SA/PAM ternary composite hydrogels

The oxygen groups of GO can interact with positively charged species like metal ions, polymers, and biomolecules, *etc.*[48–50] Meanwhile, GO itself has a huge surface area, good chemical stability, and graphitized basal plane structure, allowing it to have strong π–π interactions with the aromatic moieties present in many organic molecule dyes.[51] A variety of water-soluble dyes were used to study the dye adsorption capacity of the GO/SA/PAM composite hydrogels (Fig. S2†). As shown in Fig. 11, the dye adsorption performance of the GSP composite hydrogels can be clearly observed by the change in depth of the dye colors.

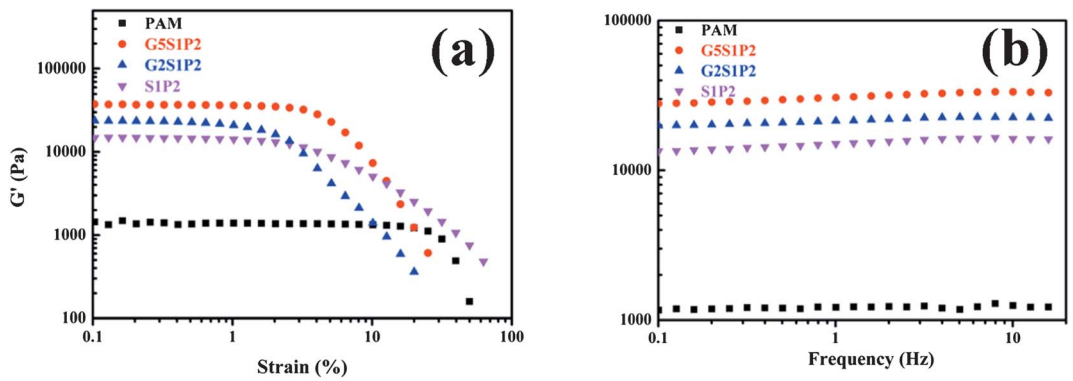

Fig. 9 Strain (a) and angular frequency (b) dependence of shear modulus (*G'*) at 25 °C for PAM, S1P2, G2S1P2 and G5S1P2 hydrogels.

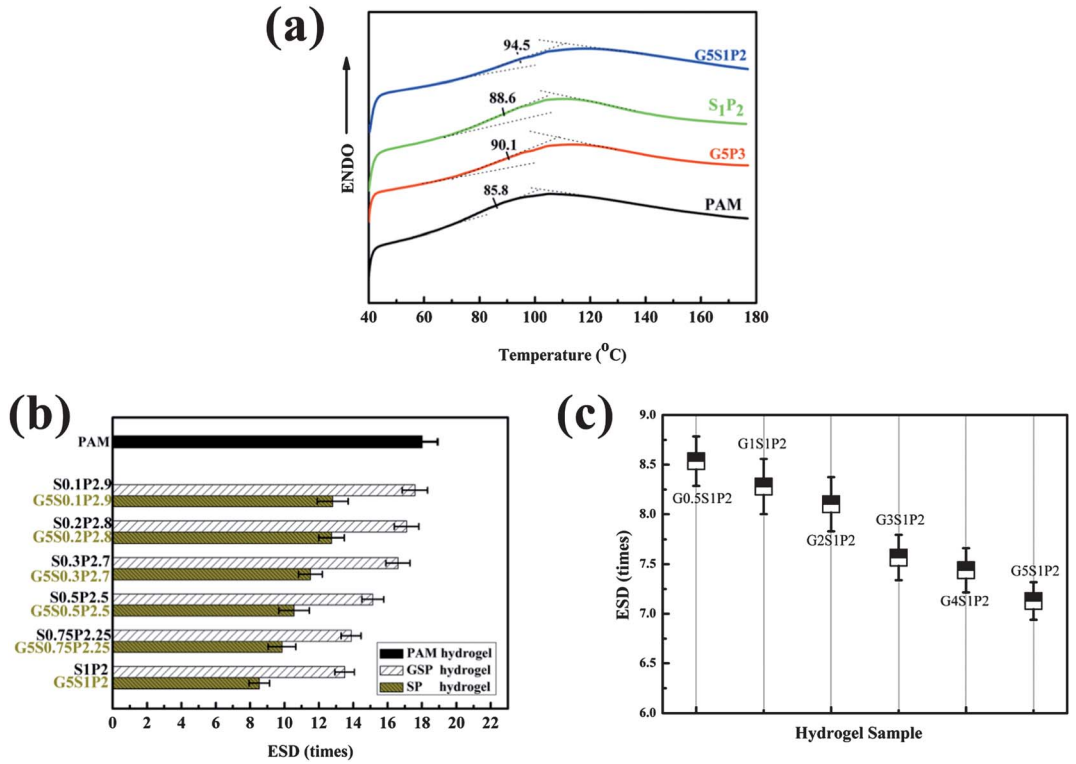

Fig. 10 (a) DSC curves of the PAM, G5P3, S1P2 and G5S1P2 hydrogels, (b) ESD of PAM, SP and GSP hydrogels and (c) ESD of the GS1P2 hydrogels with different amounts of GO.

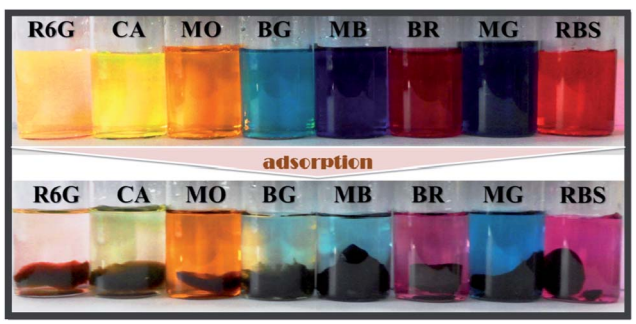

Fig. 11 Photographs of different dye solutions before and after adsorption by the GO/SA/PAM composite hydrogels.

Table 2 The adsorption capacities of the S1P2 and G5S1P2 hydrogel

Dye sample	M_w (g mol^{-1})	λ_{max} (nm)	Adsorption capacity, Q_e (mg g^{-1})	
			S1P2 hydrogel	G5S1P2 hydrogel
R6G	479.0	525	0.97538	3.71593
MB	373.9	662	0.78591	2.62483
CA	622.6	492	0.15663	4.75778
BR	502.4	521	0.49278	2.43544
MO	327.3	463	0.08893	1.24536
MG	364.9	616	0.51392	2.23856
RB	1072.8	548	1.13094	6.22738
BG	482.6	625	0.97828	5.61032

Since PAM is a nonionic polymer, the PAM hydrogel did not absorb any dye from the aqueous solution. But for the S1P2 hydrogel, it exhibited certain adsorption capacities towards to the eight kinds of dyes as shown in Table 2. Therefore, it can be inferred that the number of ionizable groups in the S1P2 hydrogel were produced after the incorporation of SA into acrylamide. With addition of GO, the adsorption capacities of the hydrogels increased sharply for the cationic dyes (R6G, MB, MG, and BG) and anionic dyes (CA, MO, BR and RB). There are covalent and non-covalent adsorptions of dyes for GO-based composite hydrogels. On the one hand for the cationic dyes (R6G, MB, MG, and BG), they contain several active points such as amino and azo groups, which interact with carboxylic groups in the hydrogels, on the other hand there are strong π–π interactions with the aromatic moieties present in the molecules of the dyes. With the introduction of GO, the GO-based composite hydrogel can be widely used for dye adsorption.

4 Conclusion

In conclusion, GO nanosheets were used as reinforcing fillers for further enhancing the mechanical performance of SP hydrogel. A series of GSP ternary composite hydrogels were successfully prepared by *in situ* polymerization followed by ionically crosslinking of calcium ions. The GO nanosheets acted as fresh chemical crosslinking points in hydrogel formation. With 5 wt% of GO, the compressive strength at 70% of strain and tensile strength of the G5S1P2 hydrogel can achieve

at ~1.543 MPa and 201.7 kPa. Meantime, the GSP ternary nanocomposite hydrogels also exhibit good elasticity. This is attributed to the strong interfacial interactions between GO nanosheets and polymer chains. FTIR and XPS spectra demonstrated the hydrogen bonding interactions between the N–H bond of PAM and O–H bond of GO nanosheets. Due to the introduction of GO, the GO/SA/PAM composite hydrogels exhibit good adsorption capacities for the cationic dyes (R6G, MB, MG, and BG) and anionic dyes (CA, MO, BR and RB). The mechanically strong GO/SA/PAM ternary nanocomposite hydrogels can be expected to widen the applications in drug delivery systems and bioengineering.

Acknowledgements

We acknowledge support from National Nature Science Foundation of China (no. 50973062). We are also grateful to Yan Wang (Ph.D.) in state key laboratory for modification of chemical fibers and polymer materials, Donghua University for his help in rheological property measurement.

References

1 A. S. Hoffman, *Adv. Drug Delivery Rev.*, 2012, **64**, 18–23.
2 Y. Qiu and K. Park, *Adv. Drug Delivery Rev.*, 2012, **64**, 49–60.
3 A. M. Kloxin, A. M. Kasko, C. N. Salinas and K. S. Anseth, *Science*, 2009, **324**, 59–63.
4 H. Itagaki, T. Kurokawa, H. Furukawa, T. Nakajima, Y. Katsumoto and J. P. Gong, *Macromolecules*, 2010, **43**, 9495–9500.
5 T. Nakajima, H. Furukawa, Y. Tanaka, T. Kurokawa, Y. Osada and J. P. Gong, *Macromolecules*, 2009, **42**, 2184–2189.
6 A. Nakayama, A. Kakugo, J. P. Gong, Y. Osada, M. Takai, T. Erata and S. Kawano, *Adv. Funct. Mater.*, 2004, **14**, 1124–1128.
7 Y. Tanaka, J. P. Gong and Y. Osada, *Prog. Polym. Sci.*, 2005, **30**, 1–9.
8 Y. Liu, M. Zhu, X. Liu, W. Zhang, B. Sun, Y. Chen and H.-J. P. Adler, *Polymer*, 2006, **47**, 1–5.
9 X. Tong, J. Zheng, Y. Lu, Z. Zhang and H. Cheng, *Mater. Lett.*, 2007, **61**, 1704–1706.
10 R. Dash, M. Foston and A. J. Ragauskas, *Carbohydr. Polym.*, 2013, **91**, 638–645.
11 Y. Zhu, S. Murali, W. Cai, X. Li, J. W. Suk, J. R. Potts and R. S. Ruoff, *Adv. Mater.*, 2010, **22**, 3906–3924.
12 S. Stankovich, D. A. Dikin, R. D. Piner, K. A. Kohlhaas, A. Kleinhammes, Y. Jia, Y. Wu, S. T. Nguyen and R. S. Ruoff, *Carbon*, 2007, **45**, 1558–1565.
13 Y. Huang, M. Zeng, J. Ren, J. Wang, L. Fan and Q. Xu, *Colloids Surf., A*, 2012, **401**, 97–106.
14 J. Shen, B. Yan, T. Li, Y. Long, N. Li and M. Ye, *Composites, Part A*, 2012, **43**, 1476–1481.
15 S. Sun and P. Wu, *J. Mater. Chem.*, 2011, **21**, 4095–4097.
16 L. Zhang, Z. Wang, C. Xu, Y. Li, J. Gao, W. Wang and Y. Liu, *J. Mater. Chem.*, 2011, **21**, 10399–10406.
17 R. Liu, S. Liang, X.-Z. Tang, D. Yan, X. Li and Z.-Z. Yu, *J. Mater. Chem.*, 2012, **22**, 14160–14167.
18 N. Zhang, R. Li, L. Zhang, H. Chen, W. Wang, Y. Liu, T. Wu, X. Wang, W. Wang, Y. Li, Y. Zhao and J. Gao, *Soft Matter*, 2011, **7**, 7231–7239.
19 Y. He, N. Zhang, Q. Gong, H. Qiu, W. Wang, Y. Liu and J. Gao, *Carbohydr. Polym.*, 2012, **88**, 1100–1108.
20 M. A. Haque, T. Kurokawa and J. P. Gong, *Polymer*, 2012, **53**, 1805–1822.
21 L. E. Rioux, S. L. Turgeon and M. Beaulieu, *Carbohydr. Polym.*, 2007, **69**, 530–537.
22 K. Y. Lee and D. J. Mooney, *Prog. Polym. Sci.*, 2012, **37**, 106–126.
23 S. K. Bajpai and S. Sharma, *React. Funct. Polym.*, 2004, **59**, 129–140.
24 J.-Y. Sun, X. Zhao, W. R. K. Illeperuma, O. Chaudhuri, K. H. Oh, D. J. Mooney, J. J. Vlassak and Z. Suo, *Nature*, 2012, **489**, 133–136.
25 W. S. Hummers and R. E. Offeman, *J. Am. Chem. Soc.*, 1958, **80**, 1339.
26 N. I. Kovtyukhova, P. J. Ollivier, B. R. Martin, T. E. Mallouk, S. A. Chizhik, E. V. Buzaneva and A. D. Gorchinskiy, *Chem. Mater.*, 1999, **11**, 771–778.
27 L. Brannon-Peppas and N. A. Peppas, *Chem. Eng. Sci.*, 1991, **46**, 715–722.
28 C. Chang, M. He, J. Zhou and L. Zhang, *Macromolecules*, 2011, **44**, 1642–1648.
29 L. Zhou, C. Gao and W. Xu, *ACS Appl. Mater. Interfaces*, 2010, **2**, 1483–1491.
30 W. Fan, W. Gao, C. Zhang, W. W. Tjiu, J. Pan and T. Liu, *J. Mater. Chem.*, 2012, **22**, 25108–25115.
31 Y. Zhou, Q. Bao, L. A. L. Tang, Y. Zhong and K. P. Loh, *Chem. Mater.*, 2009, **21**, 2950–2956.
32 D. R. Dreyer, S. Park, C. W. Bielawski and R. S. Ruoff, *Chem. Soc. Rev.*, 2010, **39**, 228–240.
33 S. Park and R. S. Ruoff, *Nat. Nanotechnol.*, 2009, **4**, 217–224.
34 C.-H. Zhu, Z.-B. Hai, C.-H. Cui, H.-H. Li, J.-F. Chen and S.-H. Yu, *Small*, 2012, **8**, 930–936.
35 N. Adrus and M. Ulbricht, *React. Funct. Polym.*, 2013, **73**, 141–148.
36 J. Shen, B. Yan, T. Li, Y. Long, N. Li and M. Ye, *Soft Matter*, 2012, **8**, 1831–1836.
37 E. C. Muniz and G. Geuskens, *Macromolecules*, 2001, **34**, 4480–4484.
38 M. Liu, W. Li, J. Rong and C. Zhou, *Colloid Polym. Sci.*, 2012, **290**, 895–905.
39 J. P. Gong, Y. Katsuyama, T. Kurokawa and Y. Osada, *Adv. Mater.*, 2003, **15**, 1155–1158.
40 P. Podsiadlo, A. K. Kaushik, E. M. Arruda, A. M. Waas, B. S. Shim, J. Xu, H. Nandivada, B. G. Pumplin, J. Lahann, A. Ramamoorthy and N. A. Kotov, *Science*, 2007, **318**, 80–83.
41 J. Zhang, H. Yang, G. Shen, P. Cheng, J. Zhang and S. Guo, *Chem. Commun.*, 2010, **46**, 1112–1114.
42 T. Çaykara, S. Demirci, M. S. Eroğlu and O. Güven, *Polymer*, 2005, **46**, 10750–10757.
43 L. Guo, H. Sato, T. Hashimoto and Y. Ozaki, *Macromolecules*, 2010, **43**, 3897–3902.

44 M. M. Coleman, D. J. Skrovanek, J. Hu and P. C. Painter, *Macromolecules*, 1988, **21**, 59–65.
45 Y. Zhang, K. L. Tan, B. Y. Liaw, D. J. Liaw and E. T. Kang, *Thin Solid Films*, 2000, **374**, 70–79.
46 Q. Tang, X. Sun, Q. Li, J. Wu and J. Lin, *Colloids Surf., A*, 2009, **346**, 91–98.
47 P. Fabbri, E. Bassoli, S. B. Bon and L. Valentini, *Polymer*, 2012, **53**, 897–902.
48 N. Zhang, H. Qiu, Y. Si, W. Wang and J. Gao, *Carbon*, 2011, **49**, 827–837.
49 G. L. Li, G. Liu, M. Li, D. Wan, K. G. Neoh and E. T. Kang, *J. Phys. Chem. C*, 2010, **114**, 12742–12748.
50 J. Liu, S. Fu, B. Yuan, Y. Li and Z. Deng, *J. Am. Chem. Soc.*, 2010, **132**, 7279–7281.
51 G. K. Ramesha, A. Vijaya Kumara, H. B. Muralidhara and S. Sampath, *J. Colloid Interface Sci.*, 2011, **361**, 270–277.